ACS APPLIED MATERIALS & INTERFACES

Research Article

www.acsami.org

Lanthanide Luminescence Enhancements in Porous Silicon Resonant Microcavities

S. N. Aisyiyah Jenie,[†] Stephanie Pace,[†] Beniamino Sciacca,[‡] Robert D. Brooks,[§] Sally E. Plush,[§] and Nicolas H. Voelcker*[,†]

[†]Mawson Institute, University of South Australia, Mawson Lakes, SA 5095, Australia

[‡]Institute for Photonics and Advanced Sensing (IPAS), School of Chemistry and Physics, The University of Adelaide, Adelaide, SA 5001, Australia

[§]Sansom Institute, School of Pharmacy and Medical Sciences, University of South Australia, Adelaide, SA 5000, Australia

Supporting Information

ABSTRACT: In this paper, the covalent immobilization and luminescence enhancement of a europium (Eu(III)) complex in a porous silicon (pSi) layer with a microcavity (pSiMC) structure are demonstrated. The alkyne-pendant arm of the Eu(III) complex was covalently immobilized on the azide-modified surface via ligand-assisted "click" chemistry. The design parameters of the microcavity were optimized to obtain an efficient luminescence-enhancing device. Luminescence enhancements by a factor of 9.5 and 3.0 were observed for Eu(III) complex bound inside the pSiMC as compared to a single layer and Bragg reflector of identical thickness, respectively, confirming the increased interaction between the immobilized molecules and the electric field in the spacer of the microcavity. When comparing pSiMCs with different resonance wavelength position, luminescence was enhanced when the resonance wavelength overlapped with the maximum emission wavelength of the Eu(III) complex at 614 nm, allowing for effective coupling between the confined light and the emitting molecules. The pSiMC also improved the spectral color purity of the Eu(III) complex luminescence. The ability of a pSiMC to act as an efficient Eu(III) luminescence enhancer, combined with the resulting sharp linelike emission, can be exploited for the development of ultrasensitive optical biosensors.

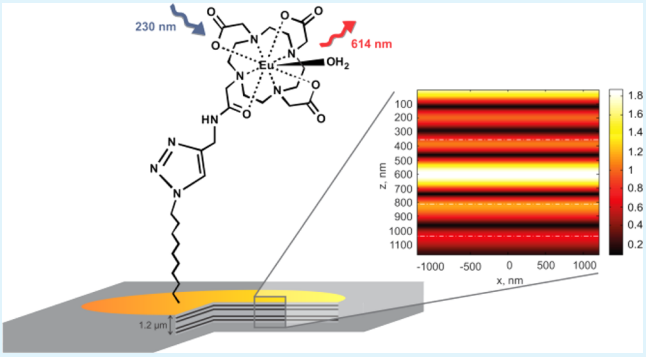

KEYWORDS: *porous silicon, microcavity, luminescence enhancement, europium, click reaction*

INTRODUCTION

Porous silicon (pSi) is a nanostructured material that can be designed to feature aligned pores running perpendicular to the surface.[1] The pores are generated by means of anodic electrochemical or photoelectrochemical etching of a silicon wafer under galvanostatic conditions in the presence of an aqueous hydrofluoric acid etchant.[2−4] By varying the etching parameters, i.e., time and current density, different optical features such as a homogeneous single layer of pores or multilayers of different pore characteristics can be produced. Multilayers of alternating high and low refractive indices contain a photonic band gap in its reflectance spectrum and are called Bragg reflectors or rugate filters depending on the transition between the layers.[1] Such photonic pSi structures have been intensively studied during the past decade for the development of optical biosensors.[5−10] One of the available photonic architectures is the optical resonant microcavity, which results when a spacer layer with certain refractive index and thickness is sandwiched between two Bragg reflectors, resulting in a "breaking" or "defect" in the multilayers stack configuration. This 1D photonic structure produces an allowed mode in the stop band, which is a narrow photonic resonance that appears as a dip in the stop band of the Bragg reflector. A spacer layer with an optical thickness of $\lambda/2$ will result in a symmetrical breaking of the stop band of the Bragg reflectors. The low reflectance of the dip in the reflectance spectrum is caused by light being trapped and absorbed in the spacer layer.[11]

It has recently been shown that the pSi microcavity (pSiMC), besides being sensitive to changes in the optical thickness of the spacer layer,[12,13] is also an excellent host-matrix for emitting materials, which permits the sharpening of the emission spectrum and amplification of the luminescence of the emitted material.[7,14−18] Setzu et al., have demonstrated that the fluorescence emission of Rhodamine 800 (LD800) at 710 nm could be enhanced by a factor of 70 if incorporated inside the pSiMC versus a pSi single layer for a certain excitation angle.[16] The optical properties of quantum dots (QD) confined inside

Received: February 17, 2014
Accepted: July 17, 2014
Published: July 17, 2014

 © 2014 American Chemical Society

an active layer of a pSi microcavity have also been studied.[17,19] The luminescence enhancement properties were compared between the single layer and the microcavity structure and found to be dependent on the structures as well as the surface chemistry of the pSi. The highest enhancement of QD luminescence was observed on thermally oxidized microcavity samples with the resonance tuned at the QD emission (i.e., 630−650 nm).[19] The fluorescence enhancement feature has also been recently observed on a more complex structure, namely a pSi coupled microcavity, which consists of two active layers that are surrounded by adjacent distributed Bragg reflectors resulting in a double resonance in the reflectance spectrum. The double resonance causes an enhancement of both the excitation and the emission of the confined fluorophore, as observed by Sciacca et al.[15] Taken together, these studies show that photonic pSiMCs can allow remarkable enhancements in the fluorescence or luminescence of an emitting substance confined in the pores.

The luminescence properties of lanthanide complexes have been intensively investigated by researchers in numerous fields including but not limited to bio- and immuoassays,[20−23] pharmaceutical applications,[24] environmental monitoring,[25] and small molecule sensing.[26,27] Lanthanide ion complexes emit at long wavelengths, with characteristic line-like emission bands (i.e., narrow emission bandwidth with sharp peaks)[23] and have long-lived luminescence lifetimes (submicroseconds to sub-milliseconds). They also possess Stoke shifts[23,28] as large as 200 nm.[29] The latter characteristic contributes to a low background signal caused by the scattered light during excitation and avoids any overlapping between the excitation and emission spectra, which is often seen in the spectra of organic fluorescent dyes. As the lanthanide ions themselves have low extinction coefficients due to Laporte forbidden f−f transitions, organic ligands with an incorporated chromophore (antenna) that have good-to-high extinction coefficients are commonly used to achieve indirect excitation of the lanthanide excited states by sensitization.[30,31] In recent years, many of the studies involving the application of the visible emitting lanthanide ion, Eu(III), include incorporating these Eu(III) complexes into a stable rigid host matrix such as a sol−gel matrix,[24,32] polymers,[33] and hydrogels.[27] Europium salts have also been impregnated into pSi films;[34] however, this report did not exploit the optical properties of pSi.

In this work, we utilized Eu(III) complexed with a cyclen (1,4,7,10-tetraazacyclododecane) with an alkyne-terminated pendant arm (Figure 1) of which the synthesis is reported elsewhere.[35] The alkyne allowed covalent attachment of the Eu(III) complex on an azide-functional pSi surface via Cu(I)-catalyzed azide−alkyne cycloaddition, the prototype "click" chemistry.[36−39]

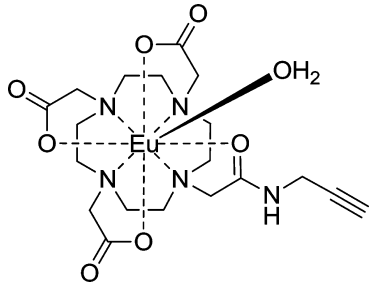

Figure 1. Eu(III)-1,4,7,10-tetraazacyclododecane-4,7,10-triacetic acid-1-(N-(prop-2-yn-1-yl) acetamide (**1**).

The main objective of this study was to obtain an efficient luminescence enhancing surface, exploiting the unique structure and properties of a pSiMC. The luminescence enhancement of the immobilized Eu(III) complex on the aligned pSiMC was demonstrated by comparing the luminescence with different pSi structures, such as single layer and Bragg reflector. We further hypothesized that in order to achieve effective enhancement of a Eu(III) complex, the pSiMC must be designed with a resonance wavelength that spectrally overlaps with the emission wavelength of the Eu(III) complex. Therefore, the luminescence enhancement for differently tuned pSiMCs modified with Eu(III) complex were compared. The resulting optimized pSiMCs could in the future be used for the design and implementation of ultrasensitive lanthanide luminescence-based biosensors.

EXPERIMENTAL SECTION

Materials. All reagents and solvents were purchased from either Sigma-Aldrich or Merck, and were used as received without any purification, unless otherwise specified. Although not strictly required, all reactions were performed under a N_2 atmosphere.

Boron doped, [100]-oriented silicon wafers (0.00055−0.001 Ω cm specific resistivity, 475−525 μm thickness) were purchased from Siltronix (France).

Preparation of pSi Thin Films. Silicon wafers were electrochemically etched in a 1:1 mixture of 48% (v/v) hydrofluoric acid (HF) (Scharlau, Australia) and ethanol (100%, ChemSupply, Australia) in a custom-built Teflon cell at 25 °C using a source meter (Keithley, USA) as the current source. Platinum mesh served as a counter electrode. The area of the exposed region of the silicon wafer was 1.767 cm^2. Prior to etching, the parasitic layer of the wafer samples was removed by etching the silicon wafers at 56.82 mA/cm^2 for 30 s, thorough rinsing with ethanol, drying under a stream of N_2 gas, and immersing it in 1 M sodium hydroxide (NaOH) for 2 min.[40] The layer was then removed and the samples were rinsed with deionized water and ethanol consecutively, before being dried under a stream of N_2 gas.

The structure of the single layer and Bragg reflectors as well as the microcavities was controlled by modulating the etching parameters, e.g., current density and etching time. The transfer matrix method-based simulation program SCOUT (W. Theiss Hard- and Software, Germany) was used to model the microcavity structure.[41] This program allows a best-fit simulation and analysis of the reflectance spectrum of the pSiMC. The software generates a theoretical reflectance spectrum of the pSi film, which is a function of the film's characteristics (dielectric function and thickness). A Bruggeman model was used to correlate the refractive index of each layer in the pSiMC to its porosity. By adjusting the free parameters of the model (e.g., porosity and layer thickness), the best-fit between the theoretical and experimental spectra were obtained.[42] It should be noted that the angular dependence of the resonance wavelength was taken into consideration in designing the pSiMC.

The microcavity structures were fabricated by etching alternating layers of high and low refractive indices (in air) of 1.4 and 2.1, respectively. The first layer of the mirror was etched at 56.8 mA/cm^2 (high porosity, H), whereas the second layer (low porosity, L) was produced at a current density of 2.8 mA/cm^2. The respective anodization times are given in Table 1. The configuration was designed at $(HL)_2$-HH-$(LH)_2$. Three types of pSiMCs with the denomination MC634, MC524 and MC660 were prepared. The numbers refer to the resonance wavelength of the microcavity in nm after modification at 45° incidence angle. Freshly etched samples were washed thoroughly with ethanol and dried under a stream of N_2 gas.

In order to obtain the same film thickness as the pSiMC (~1.2 μm), a pSi single layer was prepared by etching the silicon wafers at 56.82 mA/cm^2 for 49 s then washed thoroughly with ethanol and dried

Table 1. Etching Conditions and Nanostructure Parameters (thickness and refractive index) for the ~1.2 μm Thick pSi Thin Films with Different Cross-Sectional Structures, As Well As Resonance Wavelengths for the Microcavities at Incidence Angles 0 and 45°

pSi structure	current density (mA/cm^2)	etching time (s)	thickness (nm)	refractive index	resonance wavelength at 0°	resonance wavelength at 45°
single layer	56.8	49.1	1200	1.4	na	na
Bragg reflector					na	na
H layer	56.8	5.1	109	1.4		
L layer	2.8	59.4	93	1.8		
MC634					695	634
H layer	56.8	5.1	115	1.4		
L layer	2.8	59.4	99	2.1		
MC524					631	524
H layer	56.8	4.6	111	1.4		
L layer	2.8	54.1	83	1.9		
MC660					708	660
H layer	56.8	5.4	126	1.4		
L layer	2.8	63.0	99	2.0		

Scheme 1. Functionalization of pSi Thin Film with Eu(III) Complex Using Hydrosilylation Followed by Click Chemistry

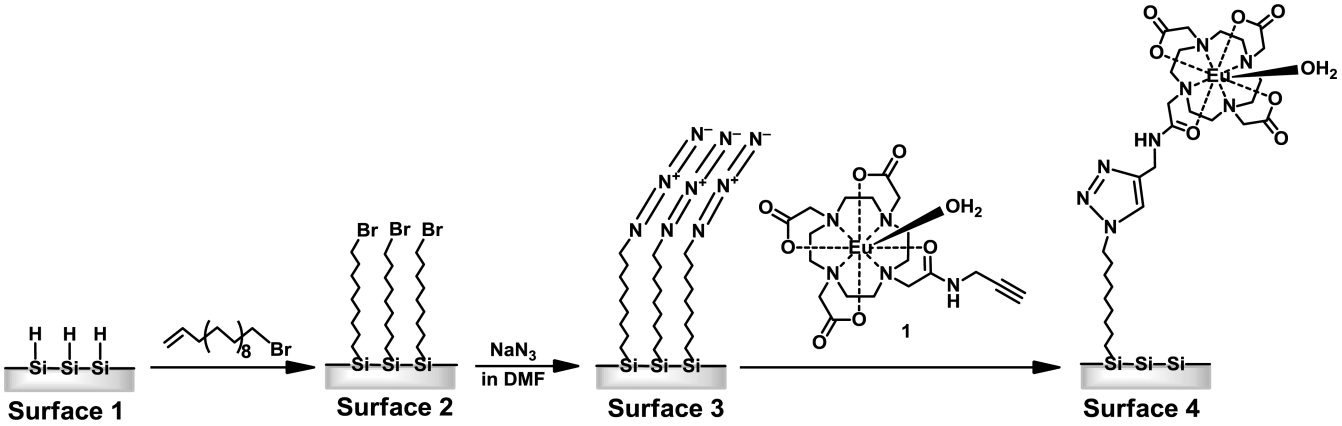

under a stream of N_2 gas. Bragg reflectors were prepared by etching alternating layers of high and low refractive indices similar to that of the pSiMCs. An anodization time of 5.1 s (for the H layer) and 59.4 s (for the L layer) was used to fabricate 5 period dielectric Bragg reflectors $(HL)_5$. Freshly etched samples were washed with ethanol and dried under a stream of N_2 gas.

Surface Modification. The modification of the porous silicon was accomplished using the three step process shown in Scheme 1. Stabilization of the surface was achieved by means of thermal hydrosilylation in neat 11-bromo-1-undecene at 120 °C for 3 h. The reaction was performed under a stream of N_2 gas. The reaction flask was then opened to the atmosphere and the functionalized surface rinsed with pure ethanol and dried under a stream of N_2 gas. The samples were then immersed in a 1 M solution of sodium azide (NaN_3) in DMF at 50 °C for 48 h and subsequently rinsed by thorough washing with DMF and ethanol and then drying under a stream of N_2 gas.

A solution of the alkyne Eu(III) complex (**1**, 1 mg/mL), ascorbic acid (0.4 mg/mL), and N,N,N′,N′-tetramethylethane-1,2-diamine (TEMED, 0.5 μL) in DMF/H_2O (1:1) were added to a reaction vial containing the azide-functionalized pSi sample, following the standard click reaction procedures.[36,38] The modified pSi sample was immersed in the above solution at room temperature for 2 min to ensure that an appropriate reducing environment was generated. The catalyst, copper(II) sulfate pentahydrate ($CuSO_4{\cdot}5H_2O$, 0.1 mg/mL, DMF: H_2O = 1:1) was then added to the mixture. The reaction was conducted at room temperature for 24 h. Afterward, the samples were rinsed with DMF, water and ethanol and then dried under a stream of N_2 gas.

Characterization. Scanning electron microscope (SEM) images were obtained on a FEI Quanta 450 Field Emission Gun Environmental SEM. The cross-sectional profiles of the pSiMC samples were measured with a 30 kV field emission source.

Interferometric reflectance spectroscopy (IRS) measurements were conducted by guiding white light from a tungsten lamp (Ocean Optics) through a fiber optic cable, which was focused through a lens onto the pSi surface at normal incidence. Light reflected from the surface was collected through the same optics and the distal end of the bifurcated fiber optic cable was connected to a CCD spectrometer (Ocean Optics S-2000). Reflectivity spectra were recorded in the wavelength range 450−1000 nm.

Fourier transform infrared (FT-IR) spectroscopy for p-type Si[100] wafers were recorded on a Bruker Hyperion 100 microscope coupled to the liquid N_2 cooled MCT detector, in the attenuated total reflectance (ATR) mode using a single-pass Germanium crystal. Background spectra were taken in air, at 3.5 cm^{-1} resolution, over the range of 650−3800 cm^{-1} and accumulating an average of 64 scans.

X-ray photoelectron spectrometry (XPS) for the chemically modified surfaces were recorded on a Specs SAGE XPS spectrometer using Mg Kα radiation source ($h\nu$ = 1253.6 eV) operating at 10 kV and 20 mA. The elements present in the sample surface were identified from a survey spectrum recorded over the energy range 0−1200 eV at a pass energy of 100 eV and a resolution of 0.5 eV and take off angle of 90° with respect to the sample surface. High resolution (0.1 eV) spectra were recorded for relevant photoelectron peaks at pass energy of 20 eV. All the binding energies (BEs) were referenced to the C 1s neutral carbon peak at 285.0 eV, to compensate for the effect of surface charging. The analysis area was circular with a diameter of 3

mm. The processing and curve-fitting of the high resolution spectra were performed using CasaXPS software.

Emission intensities of the modified surfaces were measured on a PerkinElmer LS55 luminescence spectrometer using a 230 nm excitation wavelength at a 45° angle to the surface and recording the emission over the range of 550−650 nm. The measurement was conducted in phosphorescence mode with a cycle time of 20 ms, delay time of 0.1 ms and 900 V PMT voltage.

The 2D electric field simulation of the modified microcavities were performed through MATLAB by employing rigorous coupled wave analysis (RCWA).[43] The scattering matrices of every layer were calculated and the boundary conditions at the interfaces were matched, prior to calculating the total electric field.

RESULTS AND DISCUSSIONS

Characterization of the pSi Thin Films. pSi thin films of different architectures were fabricated through a standard anodization etching technique.[44] Prior to sample preparation, the parasitic layer of the highly doped p-type silicon wafer was removed through short electrochemical etching followed by dissolution in NaOH. It has been shown that the presence of such parasitic film affects the optical quality of the photonic structure and decreases the pore sizes at the surface,[40] hindering the emitting molecules to enter the whole pSi structure.

To generate a pSiMC that efficiently enhances the emission of compound **1** (Figure 1), the Eu(III) complex molecules must infiltrate throughout the microcavity layers to interact with the enhanced electric field in the spacer. The pore size has to be large enough to facilitate this infiltration. However, the pore size parameter in turn influences porosity. Porosity is also critical for the design of pSiMC since the porosity of a layer defines its effective refractive index, which can be calculated from the Bruggeman model effective medium approximation. The refractive index contrast between alternating layers of H and L affects the photonic features of the microcavity.[45] The energy stored within the pSiMC is typically measured by its quality factor (Q-factor), which is the ratio of the central resonance wavelength and the Full width half-maximum (fwhm) of the resonance. Large Q-factors indicate small energy loss rate compared to energy stored within the microcavity, and therefore a more efficient light confinement, that pinpoints the luminescence enhancement.[46] Another important design criterion comes from the fact that compound **1** (Figure 1) absorbs at a low wavelength (230 nm). The excitation spectrum of the Eu(III) complex, **1** (see the Supporting Information, Figure S1) on the pSi surface showed high intensity below 260 nm, with an intense peak at 230 nm. This peak is attributed to the $\pi-\pi^*$ transition of the triazole moiety[47] due to immobilization of complex **1** on the surface. Since silicon has a large UV absorption coefficient, UV light passing through thick pSi multilayers is severely attenuated. This means that a balance has to be found between high Q-factor which necessitates a Bragg reflector with a high number of HL repeats and good excitation characteristics which requires thin Bragg reflector. Our simulation showed that a good trade-off between efficient excitation and efficient enhancement can be obtained for a pSiMC configuration of $(HL)_2$-HH-$(LH)_2$, which consists of two periods of Bragg reflectors and two periods of H layer as the spacer layer. Porosity of 79% (H) and 56% (L) correspond to a required current density of 56.8 and 2.8 mA/cm^2, respectively. The relating refractive indices in air were 1.4 and 2.1. The contrast between the two refractive indices or porosities resulted in a theoretical Q-value of 13 (Full width at half-maximum, fwhm of ∼54 nm). The resulting pSiMC total thickness was 1.2 μm.

Efficient enhancement of Eu(III) complex luminescence requires a good spectral alignment between the resonance wavelength of the pSiMC and the emission wavelength of the Eu(III) complex. The pSiMC samples, MC634, MC524, and MC660 were designed to have the resonance wavelength at 634, 524, and 660 nm, respectively, at 45° angle of incidence to the surface. The luminescence emission was recorded at this angle. Note that the spectral position of the features in the reflectance spectrum of a multilayer stack shifts as a function of the incidence angle: an increase in the incidence angle with respect to the normal produces a blueshift in the reflectance spectrum. The blueshift depends on the nanostructure parameters (i.e., thickness and refractive index), resonance wavelength, and incidence angle as shown in Table 1.

Figure 2 shows the measured reflectance spectrum (solid curve) and the calculated spectrum from SCOUT (dashed curve) for MC634 at normal incidence, showing a good agreement between the two. The cavity mode of a freshly etched sample at normal incidence was positioned at 695 nm with a Q-factor of 13 and a reflectance of the stop band of ∼80%, comparable to the simulation. The Q-factor of the microcavity is lower compared to that reported in previous studies that used microcavity as an emission enhancer.[7,12,17] In these studies, more than 4 repetitions of the Bragg reflectors were applied, which is in contrast to the microcavities used in this study, as they were made up of thin Bragg reflectors consisting of only 2 repetitions of the HL layer, allowing the 230 nm excitation light to enter the entire nanostructure. Therefore, the fwhm of the cavity mode broadens and thus decreases the Q-factor.

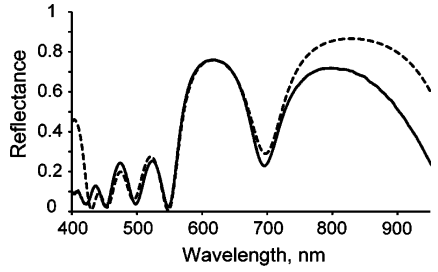

Figure 2. Reflectance spectrum of the fresh etched MC634 sample (solid curve) compared to the calculated reflectance spectrum (dashed curve) at normal incidence.

The SEM images in Figure 3 show the top view images of the high porosity (H) layer, low porosity (L) layer, and the cross-sectional view of sample MC634. Images a and b in Figure 3 were measured by preparing single layers of 56.8 and 2.8 mA/cm^2, respectively. Both figures confirmed that the pore sizes were in the range of 40−60 nm for the H layer and 8−10 nm for the L layer. This range of pore size is sufficient to allow the infiltration of the Eu(III) molecules (diameter ∼1.2 nm). Figure 3c shows that the microcavity is indeed ∼1.2 μm thick and features the desired $(HL)_2$-HH-$(LH)_2$ structure.

Eu(III) Immobilization via "Click" Chemistry. Immobilization of Eu(III) complex **1** on the pSi surface was performed through ligand-assisted alkyne−azide cycloaddition or click chemistry. The different steps of the surface functionalization were characterized by FTIR in ATR mode. Figure 4 shows the FTIR spectra for (a) a fresh etched pSi film (Scheme 1, surface

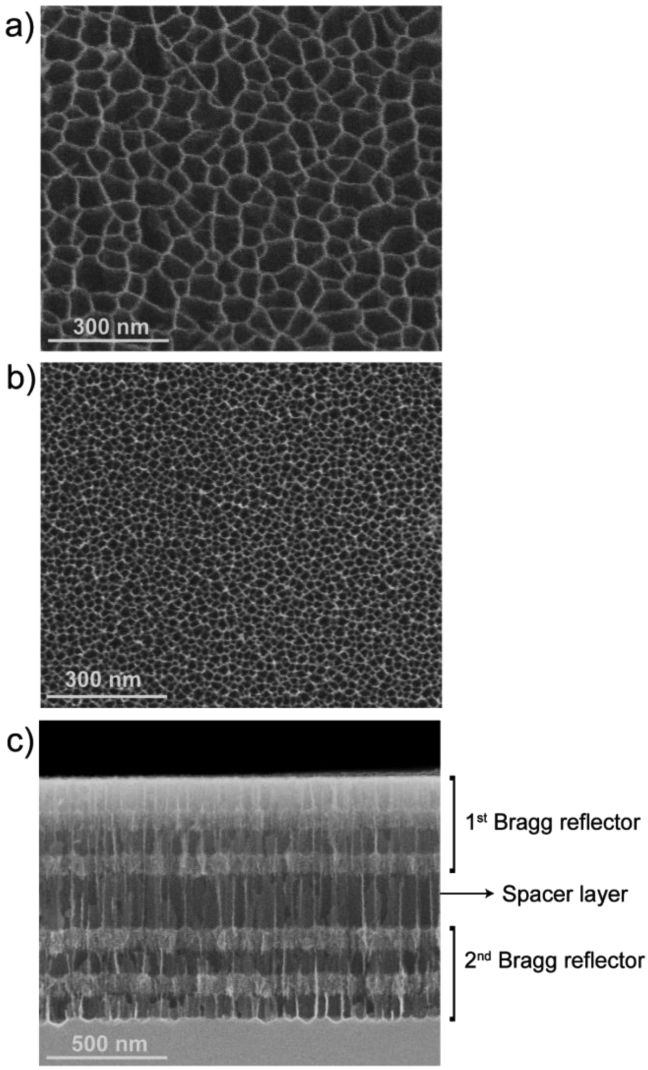

Figure 3. SEM micrographs of (a) top-view H surface, 56.8 mA/cm^2, (b) top-view L surface, 2.8 mA/cm^2, and (c) cross-sectional view of the pSiMC.

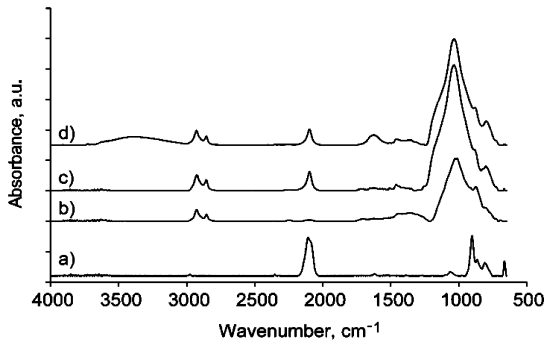

Figure 4. ATR FTIR spectra of (a) fresh etched pSi, surface 1; (b) modified pSi after hydrosilylation, surface 2; (c) after reaction with sodium azide, surface 3; and (d) after click reaction with the alkyne Eu(III)-complex **1**, surface 4.

1), (b) the same pSi film thermally hydrosilylated with 11-bromo-1-undecene (Scheme 1, surface 2), (c) after the reaction with sodium azide (Scheme 1, surface 3), and (d) after the click reaction with the alkyne-pendant Eu(III) complex (Scheme 1, surface 4). Spectrum a exhibits bands at 2100 cm^{-1}, assigned to the Si−H stretching mode. After the thermal hydrosilylation with the 11-bromo-1-undecene, bands are observed in spectrum b at 2896 and 2942 cm^{-1} that are due to the -ν_{CH2} stretching vibrational mode of a CH_2. In addition, the large band centered at 1085 cm^{-1} is attributed to the SiO stretching vibrational mode in O−Si−O, indicating that some silicon hydride sites were oxidized during the reaction forming the silicon oxide as a side product.[42]

After the nucleophilic substitution of sodium azide with the bromine-terminated surface, spectrum c presents band at 2119 cm^{-1}, assigned to the $-N_3$ stretching vibrational mode, confirming the formation of the 1-azido-undecane on the surface (surface 3).[38] The $-CH_2$ vibrations remained at the same position signifying that the aliphatic carbon chain maintained its properties on the surface and did not degrade. The intensity increase of the band centered at 1085 cm^{-1} can be explained by an overlapping of the bands associated with the stretching vibrational mode of O−Si−O and the C−N.

Following the click reaction involving the alkyne-pendant compound **1** in the presence of Cu(I) and TEMED, distinct spectral changes in spectrum d were observed, specifically the appearance of a broad peak centered at 1658 cm^{-1} corresponding to the ν(C═C) band of the triazole ring, as well as the amide (N−H) vibrational mode at 1625 cm^{-1} [48] and the carbonyl (C═O) stretching vibrational mode at 1710 cm^{-1} corresponding to compound **1**. The ATR-IR spectrum of surface 4 in the range of 1400 to 1800 cm^{-1} is shown in Figure S2 in the Supporting Information. The results show that the click reaction had occurred but that unreacted azide groups remained on the surface. Previous reports conducted by Brooks and co-workers displayed yields as low as 18% for the reaction of compound **1** with azido-mannose residue via click reaction. The interaction between the carboxylic pendant arms of compound **1** with the copper catalyst could possibly interfere the formation of a triazole ring resulting in low yield.[35] Click reaction conducted at higher temperatures (i.e., 70 °C) without the presence of Cu(I) catalyst has been reported to yield higher conversion of alkyne compound on the azide terminated surface, although under these conditions two isomers of the 1,2,4-triazole ring were formed, reducing the regioselectivity of the click reaction.[38] We have attempted conducting the click reaction at higher temperature; however, our results showed much lower emission intensity from the modified pSi compared to that from a sample prepared via click chemistry at room temperature.

Investigations using XPS were performed on the modified surfaces to provide further evidence of the substitution of bromine to azide and the attachment of Eu(III)complex on the surface. The thermal hydrosilylation of the fresh etched surface with 11-bromo-1-undecene resulted in a pronounced peak for Br(3p) at 70.5 eV for surface 2 (Figure 5a). After reaction of surface 2 with NaN_3, surface 3 showed no Br(3p) peak (Figure 5a) together with N(1s) peaks (Figure 5b), which confirmed that the reaction had occurred. The high-resolution spectrum showed that the N(1s) peak was split, with maxima at 401.0 and 405.2 eV indicating the different nitrogen atoms in the azide group.[49] Reaction of the azide terminated surface with the Eu(III) complex through click reaction was confirmed through the presence of a Eu(3d) peak at 1136.0 eV for surface 4 (Figure 5c). Moreover, the N(1s) spectral region for surface 4 (Figure 5b) displayed a lower intensity of the peak at 405.2 eV and a broad peak at 401.0 eV, as expected upon partial reaction of the surface azides to form 1,2,3-triazole groups.[49] The XPS

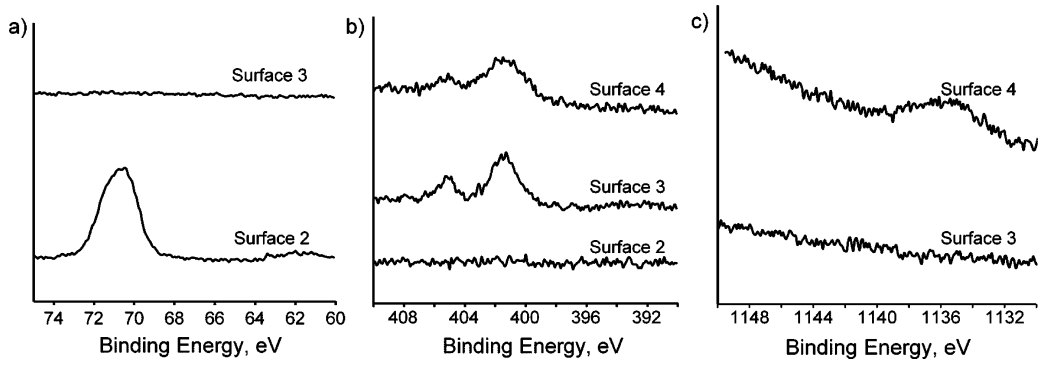

Figure 5. High-resolution elemental XPS spectra for (a) bromine, Br(3p), (b) nitrogen, N(1s) and (c) europium, Eu(3d5) region on the modified pSi surfaces.

data therefore confirm the formation of the triazole ring, observed previously by FTIR-ATR.

Investigation of Luminescence Enhancements. To tune the position of the resonance wavelength of the functionalized microcavity to the maximum emission of the Eu(III)-complex (614 nm), besides adjusting the thickness of each layer, the shift of the resonance wavelength after each chemical modification step of the surface had to be taken into account. The attachment of molecules inside the pSiMC and the surrounding Bragg reflectors produced a change of the effective refractive index of the layers, causing a shift of the resonance wavelength. Figure 6 shows the evolution of the reflectance spectra of MC634 in air at each stage of the surface functionalization process, measured at normal incidence. The optical response of the microcavity structure was measured in order to assess its optical quality, as well as defining the position of the cavity mode after each modification step. Initially, a redshift of ~35 nm from the freshly etched sample (surface 1) was observed for surface 2 (Figure 6b), confirming the increase in optical thickness due to the formation of an organic monolayer in the porous matrix. Next, the exchange of bromine with azide resulted in a blue shift of ~30 nm (Figure 6c), which may be explained by oxidation of the surface, accompanying the bromine-azide substitution reaction as seen in the IR spectra in Figure 4. The reflectance spectrum obtained from an oxidized pSi sample is typically blue-shifted from the original spectrum.[50] Finally, a red shift of ~21 nm on surface 4 further confirms the immobilization of **1** (Figure 1) inside the layers of the microcavity. The large wavelength shift of over 10 nm after each modification step is expected due to the small pore sizes of the structure, ranging from 8 to 60 nm, which is the distribution for both H and L layers. Ouyang and co-workers[12] has reported that the pore size is in inverse correlation with the shift of the cavity mode. For a given change of refractive index, small pore size or mesoporous structures would lead to higher wavelength shift compared to macroporous microcavities, thus a mesoporous surface would produce a more prominent optical response or increased sensitivity.

The final position of the resonance wavelength of surface 4 for MC634 was measured at 712 nm at normal incidence (Figure 6d). At 45° incidence, the resonance wavelength blueshifts and overlaps with the emission of compound **1**. Two offset microcavity samples (MC524 and MC660) were designed by varying the thickness of the layers, in order to demonstrate the luminescence enhancement effect of the

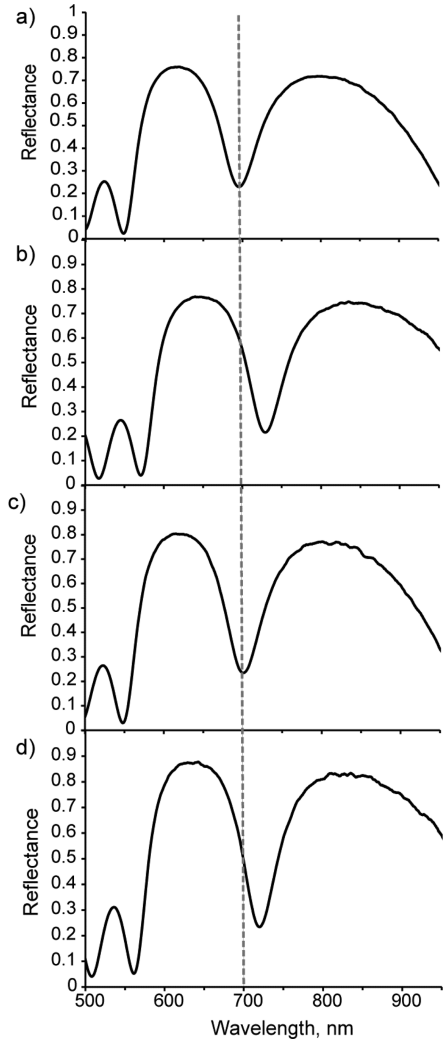

Figure 6. Reflectance spectra of sample MC634 after the surface modification steps shown in Scheme 1 at normal incidence (a) surface 1, (b) surface 2, (c) surface 3, and (d) surface 4.

correctly tuned microcavity. The optical responses of these samples are shown in Figure S3 in the Supporting Information.

The europium ion in a complex form has coordination numbers of eight or nine.[51] As shown in Figure 1 and Scheme 1, a water molecule is coordinated on the Eu(III) complex, **1**. The presence of an OH oscillator indeed influences the luminescence intensity and lifetime of the lanthanide complex.

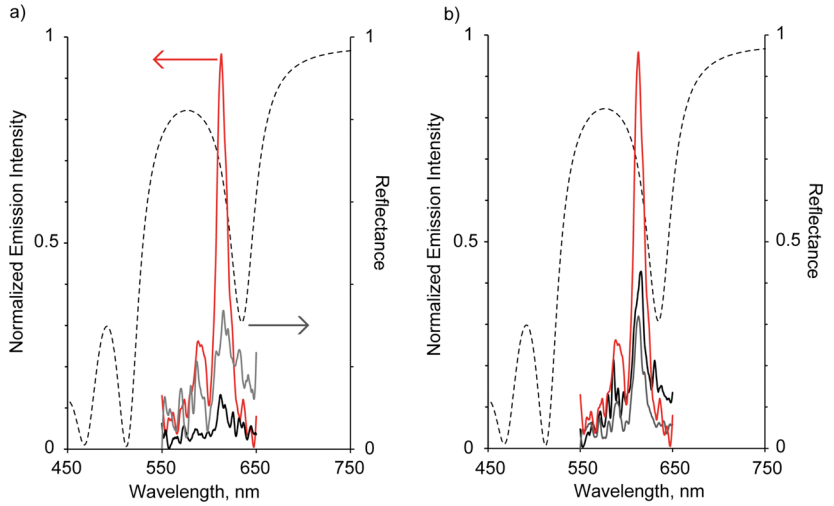

Figure 7. Luminescence spectra of the pSi films (~1.2 μm thick) functionalized with compound **1** (Figure 1). The spectra correspond to the (a) emission of MC634 (red) compared to single layer (black) and Bragg reflector (gray); (b) emission of MC634 (red) compared to MC524 (black) and MC660 (gray). The emission spectra are overlaid with the calculated reflectance spectrum of the MC634 functionalized with compound **1** at 45° incidence angle (dashed curve).

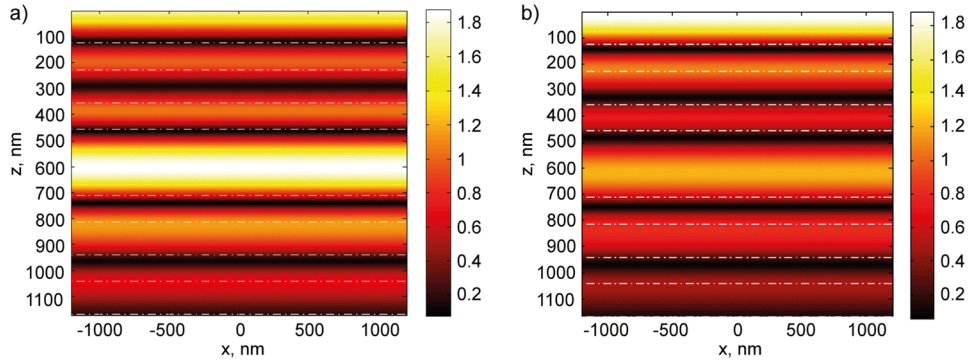

Figure 8. Electric field distribution for the modified MC634 at (a) 614 nm and (b) 585 nm with 45° incidence angle. The *z*-axis is perpendicular to the microcavity surface. The dashed white lines represent the boundary between adjacent layers.

Therefore, the number of coordinated waters, H_2O, in the complex and the luminescence lifetime of the Eu(III) complex needs to be determined.[52] Previous work conducted by Brooks et al. (2013) have calculated the number of the coordinated waters on the Eu(III) complex, **1**, using the following equation

$$q = A_{\ln}\left[\left(\frac{1}{\tau_{H2O}}\right) - \left(\frac{1}{\tau_{D2O}}\right) - B_{\ln}\right]$$

where τ_{H2O} and τ_{D2O} are the luminescence lifetimes of the complex observed in H_2O and D_2O, respectively, and A_{Ln} and B_{Ln} are constants for a given lanthanide and solvent system. The luminescence lifetimes of complex **1** at neutral pH were 0.603 and 2.091 ms in H_2O and D_2O, respectively, giving a *q*-value of 0.97.[47] This confirms that there is one coordinated water in the complex which is bound to the europium ion forming a nine coordinate complex. The luminescence of Eu(III) complex, **1**, however, was still observed even with the presence of the coordinated water. Therefore, the coordinated water was expected to remain in place and the triazole functionality was used as an antenna upon clicking the complex to the surface. The luminescence of Eu(III) complex within the pSi samples was compared between the aligned microcavity, MC634 and other pSi structures of identical thickness. To do so, we covalently attached complex **1** to the pSiMC (MC634), the single layer and the corresponding Bragg reflector by reacting all the azide-terminated samples with 1 mg/mL solutions of **1** under identical conditions. Figure 7a shows a plot of the measured emission of compound **1** from the three surfaces overlaid with the simulated reflectance spectrum of MC634 after immobilization (surface 4). This particular reflectance spectrum was calculated by performing the best fit of the measured reflectance spectrum at normal incidence for surface 4, and by using the calculated effective refractive indices of the layers for generating the correspondent spectrum at 45° incidence. The results presented in Figure 7a show that MC634 has a 9.5 and 3-fold higher emission intensity compared to single layer and Bragg reflector, respectively. This demonstrates that the resonant cavity indeed produces an enhancement of luminescence compared to nonresonant structures, because of light confinement within the spacer, contributing to higher emission intensity (see the Supporting Information, Figure S4, for the electric field distributions of freshly etched samples). This result is in agreement with previous studies where a microcavity structure amplifies the emission intensity of the confined quantum dots and FITC labeled molecules.[7,15] Narrowing of the emission spectrum compared to that of compound **1** in solution was not observed because of the smaller emission bandwidth of compound **1** (fwhm ~20 nm) with respect to the microcavity structure (fwhm of ~54 nm).

In a second set of experiments, the effect of resonance wavelength alignment with the emission maximum of the lanthanide complex was investigated. We compared MC634 with the two pSiMCs, MC524 and MC660 (functionalized with compound **1**), which had blue- and red-shifted resonances, respectively, compared to the Eu(III) emission. According to Figure 7b, all three samples showed emission maxima at 614 nm, but MC634 gave 3- and 2.4-fold higher emission intensity compared to MC524 and MC660, respectively. This further confirms that in addition to the microcavity configuration, good spectral alignment of the resonance wavelength of the pSiMC with the emission of the emitting molecule is important to achieve efficient luminescence enhancements. The reason for this enhancement can be visually analyzed in Figure 8a, where a 2D map of the electric field intensity within the MC634 microcavity after modification with the Eu(III)-complex is presented. The electric field intensity within the spacer reaches a value of almost 2 times that in free space, explaining the observed enhancement effect of the resonant microcavity. It is known that the rate of spontaneous emission of a dipole depends on its photonic environment. Having an emissive molecule, the Eu(III) complex, inside the spacer layer would allow the enhancement of spontaneous emission, and it is related to the local density of optical states at its emission wavelength, known as the Purcell effect.[53] The Purcell effect determines the ability of the microcavity to store energy at its resonance wavelength, and this is proportional to the electric field square at that wavelength.[54] The increased electric field intensity of MC634 at the emission wavelength as shown in the 2D electric field mapping in Figure 8, clarifies the enhancement in luminescence in the case of the Eu(III) complex immobilized in the MC634 cavity. The electric field maps at 614 nm for the detuned microcavity (MC524 and MC660) are shown in the Supporting Information (Figure S5).

Luminescence enhancement of the Eu(III) complex on the porous silicon surface was also observed compared to that in the solution. The luminescence of Eu(III) complex **1** in solution exhibits five emission bands ($^5D_0 \rightarrow {}^7F_J$, $J = 0-4$) as shown in Figure S6 in the Supporting Information. The most prominent emission bands that contributes to the emission of the Eu(III) complex, are the ones originating from the $^5D_0 \rightarrow {}^7F_1$ ($\lambda = 585$ nm) and the $^5D_0 \rightarrow {}^7F_2$ ($\lambda = 614$ nm) transitions. Table 2 shows the intensity ratio of $^5D_0 \rightarrow {}^7F_2$ to $^5D_0 \rightarrow {}^7F_1$ of compound **1** in solution and bound to the pSi surface. This ratio is indicative of the spectral color purity of the luminescence of Eu(III), with a higher ratio showing an increased purity of the emission. Color purity is regarded as an important parameter in studies related to the luminescence properties of lanthanides[55] considering that these ions produce emissions at five different wavelengths. Here, the luminescence of complex **1** immobilized in the pSi surface caused an increase of the $^5D_0 \rightarrow {}^7F_2$ to $^5D_0 \rightarrow {}^7F_1$ ratio. Both the $^5D_0 \rightarrow {}^7F_1$ and $^5D_0 \rightarrow {}^7F_2$ transitions are prone to changes in the host environment; however, the sensitivity and susceptibility differ. The $^5D_0 \rightarrow {}^7F_1$ transition is susceptible to magnetic dipole transitions, whereas the electrons energy transitions of the $^5D_0 \rightarrow {}^7F_2$ are profoundly dependent on the local coordination of the Eu(III) complex environment.[33,55] The lack of change in the $^5D_0 \rightarrow {}^7F_1$ intensity indicates that the concentration differences between the porous silicon surfaces are minimal. The increase in the $^5D_0 \rightarrow {}^7F_2$ to $^5D_0 \rightarrow {}^7F_1$ ratio suggests that there is a change in the coordination environment of the Eu(III) ion as a consequence of the Eu(III) complex binding on the surface. We suggest that the so-called "second-sphere" coordination of the Eu(III) complex, which occurs in the solution phase where a hydrogen bond acceptor brings closer an unbound water molecule to the Eu(III),[56,57] was altered upon attachment of the complex on the hydrophobic pSi surface, hence the ratio of $^5D_0 \rightarrow {}^7F_2$ to $^5D_0 \rightarrow {}^7F_1$ was higher on the solid surface compared to that in solution.

The pSiMC with aligned resonance wavelength (MC634) gave the highest $^5D_0 \rightarrow {}^7F_2$ to $^5D_0 \rightarrow {}^7F_1$ ratio (4.0) of all the other pSi structures investigated, as shown in Table 2. The increased ratio could possibly be caused by the effect of the density of optical states. The emission at 585 nm is hindered by the presence of the stop band from the reflectance spectrum of MC634, as can be seen in Figure 7. This indicates that there are no or very few optical states available for the emission originating from the $^5D_0 \rightarrow {}^7F_1$ transition or in other words the MC634 "blocks" the 585 nm emission as shown in Figure 8b. This further confirms that having both a spacer layer in the multilayer structure and establishing an overlap of the resonance wavelength of the microcavity with the emission of Eu(III)-complex will generate an efficient luminescence enhancement platform.

Table 2. Ratios of Luminescence Intensity of $^5D_0 \rightarrow {}^7F_2/{}^5D_0 \rightarrow {}^7F_1$ for Compound 1 in Solution and Incorporated on pSi Thin Films

	$^5D_0 \rightarrow {}^7F_2/{}^5D_0 \rightarrow {}^7F_1$
50 μM solution of 1 in DMF/H_2O (1:1,v/v)	1.2
On pSi thin films:	
single layer	3.6
Bragg reflector	1.6
MC634	4.0
MC524	2.1
MC660	3.0

CONCLUSION

The investigation of luminescence properties of a Eu(III) complex immobilized on different structures of pSi (i.e., single layer, Bragg reflector, and microcavity) of the same thickness revealed that the pSiMC with resonance wavelength overlapping with the emission maximum of the Eu(III) complex gave a greater than 3-fold luminescence enhancement over the other structures. Fine tuning of the pores sizes, thickness of Bragg reflector layers of pSiMC, resonance wavelength and excitation light through the pSi layer proved to generate an optimum configuration of the microcavity. The ligand-assisted "click" reaction was presented as an effective mechanism for attaching the alkyne pendant-arm of the Eu(III) complex to an azide modified surface, which was obtained in a two-step surface modification procedure. The success of the surface functionalizations was confirmed by FTIR- ATR, XPS and IRS. The pSiMC gratifyingly also served as an efficient host material for improving the luminescence quality, i.e., spectral color purity, of the Eu(III) complex. We believe that this study will serve as the basis for future studies where the emission enhancement of the confined Eu(III) complexes in porous silicon microcavities will facilitate the development of luminescent biosensors or biosensor arrays.

■ ASSOCIATED CONTENT

Supporting Information

Excitation spectrum of Eu(III)-complex (**1**) on pSi surface, ATR-IR spectra of Eu(III)-complex (**1**) modified surface (Surface 4), optical response of MC524 and MC660, electric field distributions of the freshly etched pSi samples (i.e., single layer, Bragg reflector, and microcavities), 2D electric field mapping of MC524 and MC660, and luminescence spectrum of Eu(III)-complex (**1**) in solution phase (PDF). This material is available free of charge via the Internet at http://pubs.acs.org.

■ AUTHOR INFORMATION

Corresponding Author

*E-mail: nico.voelcker@unisa.edu.au. Tel.: +61 8 8302 5508. Fax: +61 8 8302 5613.

Notes

The authors declare no competing financial interest.

■ ACKNOWLEDGMENTS

S.N.A.J. thanks the Australian Government for the Australia Award Scholarship and also acknowledges funding from the Wound Management Innovation CRC (Australia).

■ REFERENCES

(1) Zhao, Y.; Zhao, X.; Gu, Z. Photonic Crystals in Bioassays. *Adv. Funct. Mater.* **2010**, *20*, 2970−2988.

(2) Jane, A.; Dronov, R.; Hodges, A.; Voelcker, N. H. Porous Silicon Biosensors on the Advance. *Trends in Biotechnol.* **2009**, *27*, 230−239.

(3) Sailor, M. J.; Heinrich, J. L.; Lauerhaas, J. M., Luminescent Porous Silicon: Synthesis, Chemistry, and Applications. In *Studies in Surface Science and Catalysis*; Prashant, V. K., Dan, M., Eds.; Elsevier: Amsterdam, 1997; Vol. *103*, pp 209−235.

(4) Sailor, M. J.; Wu, E. C. Photoluminescence-Based Sensing with Porous Silicon Films, Microparticles, and Nanoparticles. *Adv. Funct. Mater.* **2009**, *19*, 3195−3208.

(5) Kilian, K. A.; Böcking, T.; Gaus, K.; Gal, M.; Gooding, J. J. Peptide-Modified Optical Filters for Detecting Protease Activity. *ACS Nano* **2007**, *1*, 355−361.

(6) Ruminski, A. M.; King, B. H.; Salonen, J.; Snyder, J. L.; Sailor, M. J. Porous Silicon-Based Optical Microsensors for Volatile Organic Analytes: Effect of Surface Chemistry on Stability and Specificity. *Adv. Funct. Mater.* **2010**, *20*, 2874−2883.

(7) Palestino, G.; Agarwal, V.; Aulombard, R.; Pérez, E. a.; Gergely, C. Biosensing and Protein Fluorescence Enhancement by Functionalized Porous Silicon Devices. *Langmuir* **2008**, *24*, 13765−13771.

(8) Chan, S.; Horner, S. R.; Fauchet, P. M.; Miller, B. L. Identification of Gram Negative Bacteria Using Nanoscale Silicon Microcavities. *J. Am. Chem. Soc.* **2001**, *123*, 11797−11798.

(9) Palestino, G.; Martin, M.; Agarwal, V.; Legros, R.; Cloitre, T.; Zimányi, L.; Gergely, C. Detection and Light Enhancement of Glucose Oxidase Adsorbed on Porous Silicon Microcavities. *Phys. Status Solidi C* **2009**, *6*, 1624−1628.

(10) Levitsky, I. A.; Euler, W. B.; Tokranova, N.; Rose, A. Fluorescent Polymer-Porous Silicon Microcavity Devices for Explosive Detection. *Appl. Phys. Lett.* **2007**, *90*, 041904−1−041904−3.

(11) Pavesi, L.; Mulloni, V. All Porous Silicon Microcavities: Growth and Physics. *J. Lumin.* **1998**, *80*, 43−52.

(12) Ouyang, H.; Christophersen, M.; Viard, R.; Miller, B. L.; Fauchet, P. M. Macroporous Silicon Microcavities for Macromolecule Detection. *Adv. Funct. Mater.* **2005**, *15*, 1851−1859.

(13) Weiss, S. M.; Fauchet, P. M. Electrically Tunable Porous Silicon Active Mirrors. *Phys. Status Solidi A* **2003**, *197*, 556−560.

(14) Setzu, S.; Ferrand, P.; Romestain, R. Optical Properties of Multilayered Porous Silicon. *Mater. Sci. Eng., B* **2000**, *69−70*, 34−42.

(15) Sciacca, B.; Frascella, F.; Venturello, A.; Rivolo, P.; Descrovi, E.; Giorgis, F.; Geobaldo, F. Doubly Resonant Porous Silicon Microcavities for Enhanced Detection of Fluorescent Organic Molecules. *Sens. Actuators, B* **2009**, *137*, 467−470.

(16) Setzu, S.; Létant, S.; Solsona, P.; Romestain, R.; Vial, J. C. Improvement of the Luminescence in P-Type as-Prepared or Dye Impregnated Porous Silicon Microcavities. *J. Lumin.* **1998**, *80*, 129−132.

(17) Qiao, H.; Guan, B.; Bocking, T.; Gal, M.; Gooding, J. J.; Reece, P. J. Optical Properties of Ii-Vi Colloidal Quantum Dot Doped Porous Silicon Microcavities. *Appl. Phys. Lett.* **2010**, *96*, 161106.

(18) Poitras, C. B.; Lipson, M.; Du, H.; Hahn, M. A.; Krauss, T. D. Photoluminescence Enhancement of Colloidal Quantum Dots Embedded in a Monolithic Microcavity. *Appl. Phys. Lett.* **2003**, *82*, 4032−4034.

(19) DeLouise, L. A.; Ouyang, H. Photoinduced Fluorescence Enhancement and Energy Transfer Effects of Quantum Dots Porous Silicon. *Phys. Status Solidi C* **2009**, *6*, 1729−1735.

(20) Dakubu, S.; Ekins, R. P. The Fluorometric Determination of Europium Ion Concentration as Used in Time-Resolved Fluoroimmunoassay. *Anal. Biochem.* **1985**, *144*, 20−26.

(21) Gao, X.; Hsu, C.-K.; Heinz, L. J.; Morin, J.; Shi, Y.; Shukla, N. K.; Smiley, D. L.; Xu, J.; Zhong, B.; Slieker, L. J. Europium-Labeled Melanin-Concentrating Hormone Analogues: Ligands for Measuring Binding to Melanin-Concentrating Hormone Receptors 1 and 2. *Anal. Biochem.* **2004**, *328*, 187−195.

(22) Hemmilä, I.; Dakubu, S.; Mukkala, V.-M.; Siitari, H.; Lövgren, T. Europium as a Label in Time-Resolved Immunofluorometric Assays. *Anal. Biochem.* **1984**, *137*, 335−343.

(23) Huhtinen, P.; Kivelä, M.; Kuronen, O.; Hagren, V.; Takalo, H.; Tenhu, H.; Lövgren, T.; Härmä, H. Synthesis, Characterization, and Application of Eu(Iii), Tb(Iii), Sm(Iii), and Dy(Iii) Lanthanide Chelate Nanoparticle Labels. *Anal. Chem.* **2005**, *77*, 2643−2648.

(24) Milanova, M.; Zaharieva, J.; Manolov, I.; Getzova, M.; Todorovsky, D. Lanthanide Complexes with B-Diketones and Coumarin Derivates: Synthesis, Thermal Behaviour, Optical and Pharmacological Properties and Immobilisation. *J. Rare Earths* **2010**, *28* (Supplement 1), 66−74.

(25) Wolfbeis, O. S.; Dürkop, A.; Wu, M.; Lin, Z. A Europium-Ion-Based Luminescent Sensing Probe for Hydrogen Peroxide. *Angew. Chem., Int. Ed.* **2002**, *41*, 4495−4498.

(26) Plush, S. E.; Gunnlaugsson, T. Luminescent Sensing of Dicarboxylates in Water by a Bismacrocyclic Dinuclear Eu(Iii) Conjugate. *Org. Lett.* **2007**, *9*, 1919−1922.

(27) McCoy, C. P.; Stomeo, F.; Plush, S. E.; Gunnlaugsson, T. Soft Matter Ph Sensing: From Luminescent Lanthanide Ph Switches in Solution to Sensing in Hydrogels. *Chem. Mater.* **2006**, *18*, 4336−4343.

(28) Matsumoto, K.; Yuan, J., Lanthanide Chelates as Fluorescence Labels for Diagnostics and Biotechnology. In *Metal Ions in Biological Systems: The Lanthanides and Their Interrelations with Biosystems*; Sigel, H., Ed.; CRC Press: Boca Raton, FL, 2003; Vol. *40*.

(29) Handl, H. L.; Gillies, R. J. Lanthanide-Based Luminescent Assays for Ligand-Receptor Interactions. *Life Sci.* **2005**, *77*, 361−371.

(30) Moore, E. G.; Samuel, A. P. S.; Raymond, K. N. From Antenna to Assay: Lessons Learned in Lanthanide Luminescence. *Acc. Chem. Res.* **2009**, *42*, 542−552.

(31) Carlos, L. D.; Ferreira, R. A. S.; Bermudez, V. d. Z.; Ribeiro, S. J. L. Lanthanide-Containing Light-Emitting Organic−Inorganic Hybrids: A Bet on the Future. *Adv. Mater.* **2009**, *21*, 509−534.

(32) Wang, F.; Fan, X.; Wang, M.; Zhang, X. Luminescence Behavior of the Dibenzoyl Methane Europium(Iii) Complexes in Sol−Gel Derived Host Materials. *J. Lumin.* **2005**, *114*, 281−287.

(33) Binnemans, K. Lanthanide-Based Luminescent Hybrid Materials. *Chem. Rev.* **2009**, *109*, 4283−4374.

(34) Moadhen, A.; Elhouichet, H.; Oueslati, M.; Férid, M. Photoluminescence Properties of Europium-Doped Porous Silicon Nanocomposites. *J. Lumin.* **2002**, *99*, 13−17.

(35) Brooks, R.; Du, Z.; Borlace, G.; Brooks, D.; Plush, S. E. Synthesis and Characterisation of First Generation Luminescent Lanthanide Complexes Suitable for Being Adapted for Uptake Via the Mannose Receptor. *J. Inorg. Chem.* **2013**, *2013*, 1−9.

(36) Ciampi, S.; Böcking, T.; Kilian, K. A.; Harper, J. B.; Gooding, J. J. Click Chemistry in Mesoporous Materials: Functionalization of Porous Silicon Rugate Filters. *Langmuir* **2008**, *24*, 5888−5892.
(37) Ciampi, S.; Böcking, T.; Kilian, K. A.; James, M.; Harper, J. B.; Gooding, J. J. Functionalization of Acetylene-Terminated Monolayers on Si(100) Surfaces: A Click Chemistry Approach. *Langmuir* **2007**, *23*, 9320−9329.
(38) Lummerstorfer, T.; Hoffmann, H. Click Chemistry on Surfaces: 1,3-Dipolar Cycloaddition Reactions of Azide-Terminated Monolayers on Silica. *J. Phys. Chem. B* **2004**, *108*, 3963−3966.
(39) Bock, V. D.; Hiemstra, H.; van Maarseveen, J. H. Cui-Catalyzed Alkyne−Azide "Click" Cycloadditions from a Mechanistic and Synthetic Perspective. *Eur. J. Org. Chem.* **2006**, *2006*, 51−68.
(40) Sciacca, B.; Secret, E.; Pace, S.; Gonzalez, P.; Geobaldo, F.; Quignard, F.; Cunin, F. Chitosan-Functionalized Porous Silicon Optical Transducer for the Detection of Carboxylic Acid-Containing Drugs in Water. *J. Mater. Chem.* **2011**, *21*, 2294−2302.
(41) Francia, G. D.; Ferrara, V. L.; Manzo, S.; Chiavarini, S. Towards a Label-Free Optical Porous Silicon DNA Sensor. *Biosens. Bioelectron.* **2005**, *21*, 661−665.
(42) Pace, S.; Vasani, R. B.; Cunin, F.; Voelcker, N. H. Study of the Optical Properties of a Thermoresponsive Polymer Grafted onto Porous Silicon Scaffolds. *New J. Chem.* **2013**, *37*, 228−235.
(43) Moharam, M. G.; Grann, E. B.; Pommet, D. A.; Gaylord, T. K. Formulation for Stable and Efficient Implementation of the Rigorous Coupled-Wave Analysis of Binary Gratings. *J. Opt. Soc. Am. A* **1995**, *12*, 1068−1076.
(44) Tinsley-Bown, A. M.; Canham, L. T.; Hollings, M.; Anderson, M. H.; Reeves, C. L.; Cox, T. I.; Nicklin, S.; Squirrell, D. J.; Perkins, E.; Hutchinson, A.; Sailor, M. J.; Wun, A. Tuning the Pore Size and Surface Chemistry of Porous Silicon for Immunoassays. *Phys. Status Solidi A* **2000**, *182*, 547−553.
(45) Chan, S.; Fauchet, P. M.; Li, Y.; Rothberg, L. J.; Miller, B. L. Porous Silicon Microcavities for Biosensing Applications. *Phys. Status Solidi A* **2000**, *182*, 541−546.
(46) Ouyang, H.; Fauchet, P. M. Biosensing Using Porous Silicon Photonic Bandgap Structures. *Proc. SPIE 6005, Photonic Crystals and Photonic Crystal Fibers for Sensing Applications* **2005**, 600508−600508−15.
(47) Brooks, R.; Du, Z.; Borlace, G.; Brooks, D.; Plush, S. Synthesis and Characterisation of First Generation Luminescent Lanthanide Complexes Suitable for Being Adapted for Uptake Via the Mannose Receptor. *J. Inorg. Chem.* **2013**, *2013*, 1−9.
(48) Antoni, P.; Malkoch, M.; Vamvounis, G.; Nystrom, D.; Nystrom, A.; Lindgren, M.; Hult, A. Europium Confined Cyclen Dendrimers with Photophysically Active Triazoles. *J. Mater. Chem.* **2008**, *18*, 2545−2554.
(49) Haensch, C.; Hoeppener, S.; Schubert, U. S. Chemical Surface Reactions by Click Chemistry: Coumarin Dye Modification of 11-Bromoundecyltrichlorosilane Monolayers. *Nanotechnology* **2008**, *19*, 035703.
(50) Song, J. H.; Sailor, M. J. Chemical Modification of Crystalline Porous Silicon Surfaces. *Comments Inorg. Chem.* **1999**, *21*, 69−84.
(51) Parker, D.; Williams, J. A. G. Getting Excited About Lanthanide Complexation Chemistry. *J. Chem. Soc., Dalton Trans.* **1996**, 3613−3628.
(52) Supkowski, R. M.; Horrocks, W. D., Jr On the Determination of the Number of Water Molecules, Q, Coordinated to Europium(Iii) Ions in Solution from Luminescence Decay Lifetimes. *Inorg. Chim. Acta* **2002**, *340*, 44−48.
(53) Purcell, E. M. Spontaneous Emission Probabilities at Radio Frequencies. *Phys. Rev.* **1946**, *69*, 681−681.
(54) Koenderink, A. F. On the Use of Purcell Factors for Plasmon Antennas. *Opt. Lett.* **2010**, *35*, 4208−4210.
(55) Xu, Q.; Li, L.; Li, B.; Yu, J.; Xu, R. Encapsulation and Luminescent Property of Tetrakis (1-(2-Thenoyl)-3,3,3-Trifluoracetate) Europium N-Hexadecyl Pyridinium in Modified Si−Mcm-41. *Microporous Mesoporous Mater.* **2000**, *38*, 351−358.
(56) Beeby, A.; M. Clarkson, I.; S. Dickins, R.; Faulkner, S.; Parker, D.; Royle, L.; S. de Sousa, A.; A. Gareth Williams, J.; Woods, M. Non-Radiative Deactivation of the Excited States of Europium, Terbium and Ytterbium Complexes by Proximate Energy-Matched Oh, Nh and Ch Oscillators: An Improved Luminescence Method for Establishing Solution Hydration States. *J. Chem. Soc., Perkin Trans. 2* **1999**, 493−504.
(57) Aime, S.; Botta, M.; Parker, D.; Williams, J. A. G. Extent of Hydration of Octadentate Lanthanide Complexes Incorporating Phosphinate Donors: Solution Relaxometry and Luminescence Studies. *J. Chem. Soc., Dalton Trans.* **1996**, 17−23.